Applied Catalysis B: Environmental 176–177 (2015) 513–521

Contents lists available at ScienceDirect

Applied Catalysis B: Environmental

journal homepage: www.elsevier.com/locate/apcatb

Coke-resistant Ni@SiO_2 catalyst for dry reforming of methane

Junshe Zhang, Fanxing Li *

Department of Chemical and Biomolecular Engineering, North Carolina State University, Raleigh, NC 27606, United States

ARTICLE INFO

Article history:
Received 28 November 2014
Received in revised form 11 March 2015
Accepted 17 April 2015
Available online 20 April 2015

Keywords:
Coke-resistance
Nickel oxide nanoparticles
Core–shell catalyst
Dry reforming of methane
Carbon dioxide

ABSTRACT

Nanostructured Ni@SiO_2 core–shell catalyst is prepared from nickel oxide nanoparticles by a facile method. Calcination of as-synthesized core–shell nanoparticles creates a micro/meso-porous structure in the amorphous silica shell. The catalytic performance of core–shell catalyst toward dry reforming of methane was first evaluated in a thermogravimeter coupled with a mass spectrometer. Coking is negligible in a reforming period of 40 h on stream at 850 °C, while more than 0.32 g_{coke} g_{cat}^{-1} is produced on a commercial Ni-based reforming catalyst in 6.4 h at the same reforming condition. Dry reforming was also performed in a continuous flow, fixed-bed reactor at 750 °C. Characterization of spent catalyst further confirms that Ni@SiO_2 catalyst has high coke-resistance for dry reforming. The amount of coke deposited on the core–shell catalyst in 24.5 h is 0.012 g_{coke} g_{cat}^{-1}.

1. Introduction

Dry reforming of methane (DRM) is a promising approach for carbon dioxide utilization and syngas generation ($CH_4 + CO_2 = 2CO + 2H_2$) [1]. Although the DRM concept has many environmental and economic advantages; it has yet to be commercialized. A key challenge that hinders the widespread applications of DRM resides in catalyst performance. Supported noble metal catalysts, e.g., platinum (Pt), palladium (Pd), rhodium (Rh), and ruthenium (Ru) are active and stable [2,3] but are highly expensive. In contrast, Ni-based catalysts are more attractive from an economic standpoint [4–9]. However, industrial applications of Ni catalysts in dry reforming reactions are limited due to their poor stability, caused by sintering of active metallic particles and coke deposition on the metal surfaces [8–9]. Therefore, coke formation represents a major obstacle for DRM over Ni-based catalysts.

Previous studies have indicated that coke formation is primarily catalyzed by the Ni atoms located at corners and edges of the surface [10,11]. In addition, coke formation over small Ni particles is not energetically favored. As a result, extensive efforts have been devoted to control the size of Ni particles [12,13]. To date, effective options to inhibit coke formation include poisoning coke-formation sites with sulfur, introducing alkali, alkaline earth or transition metal promoters, chemically or physically dispersing Ni in other metal oxides, confining Ni particles in mesoporous materials, and encapsulating catalyst particles in an inorganic shell [12–20]. For instance, immobilized Ni NPs in channels of SBA-15 exhibit excellent coking- and sintering-resistance [20], while coating Ni/SiO_2 particles with a silica layer can reduce coke deposition [21]. Coating metal nanoparticles (NPs) with an inorganic layer such as alumina (Al_2O_3) and silica (SiO_2) is found to effectively stabilize NPs against sintering at high temperatures while inhibiting coke formation for hydrocarbon conversion [22–25]. One may anticipate that confining Ni NPs inside a silica shell will confer high coke-resistance. Indeed, previous studies have demonstrated that porous SiO_2-coated Ni catalyst have excellent coke-resistance in the partial oxidation of methane (POM) [26,27]. Li et al. reported catalytic performance of a Ni-yolk@Ni@SiO_2 catalyst toward DRM [19], which is more prone to coke formation than POM. Although coking on this catalyst was reported to be negligible [19], this has not been confirmed by a direct measurement. Therefore, comprehensive studies are desired to further our understanding of coke formation on coated Ni NPs. Generally, the procedure to prepare core–shell particles involves synthesis of Ni NPs, which may pose some challenges for the scale-up of core–shell catalysts. In this context, we investigated CO_2 reforming of CH_4 on Ni@SiO_2 core–shell catalysts prepared by a simple and scalable method. The preparation of core–shell catalyst includes three steps: (1) dispersing NiO NPs (10–20 nm) in cetyltrimethylammonium bromide (CTAB) solution using a blender; (2) silicon alkoxide hydrolysis and condensation around NiO NPs in the presence of sodium hydroxide; (3) removing CTAB by calcination in static air. The catalytic performance was first evaluated on a thermogravimeter at 850 °C and then in a continuous flow, fixed-bed reactor at 750 °C. Both physisorption and chemisorption indicate that the Ni cores are

* Corresponding author. Tel.: +1 919 515 7328; fax: +1 919 515 3465.
E-mail address: fli5@ncsu.edu (F. Li).

http://dx.doi.org/10.1016/j.apcatb.2015.04.039
0926-3373/

accessible to gas molecules through the pores of the shell, which effectively suppresses coke deposition in DRM.

2. Experimental

2.1. Preparation of core–shell catalyst

Typically, 0.1 g NiO nanoparticles (10–20 nm, Research Nanomaterials) and 0.1 g cetyltrimethyl ammonium bromide (>99%, Sigma–Aldrich) was added to 100 cm^3 deionized water. Subsequently, they were mixed with a blender (Waring MX1200XTS, Waring Commercial) at a speed of 30,000 rpm, followed by ultrasonication for 10 min. The suspension was placed in a sealed bottle for one day to obtain a NiO dispersion. To prepare SiO_2 coated NPs, 80 cm^3 NiO suspension was placed in a beaker, to which 2 cm^3 NaOH (>98%, Sigma–Aldrich) solution (0.05 M) was added under stirring (600 rpm) to adjust the pH. The pH of dispersion, after 1 h with agitation, was between 10 and 11. Subsequently, 8 cm^3 of 10 vol.% tetraethyl orthosilicate (>99%, Sigma–Aldrich) in ethanol (>99.5%, Sigma–Aldrich) solution was added to the NiO dispersion. After the dispersion was stirred for another 10 min, it was kept in the beaker covered with parafilm at ambient conditions for two days. The dispersion was then washed and centrifuged. The resultant nanoparticles were first dried in an oven at 110 °C overnight and then calcined in static air for 2 h at 350 °C.

2.2. Characterization

N_2-physisorption was performed at −196 °C on a volumetric adsorption analyzer (Micromeritics ASAP 2020). Before the analysis, the sample was outgassed under vacuum at 300 °C for 2 h. The specific surface area was calculated by using the Brunauer–Emmett–Teller (BET) method in the relative pressure range from 3×10^{-6} to 0.2, and the pore size distribution (PSD) was estimated from the desorption branch of isotherms.

To determine the Ni content in the calcined core–shell catalysts, the catalysts were digested by 1.0 M HNO_3 (Fischer Scientific) at 100 °C for 2 h. The aliquots were filtered with a 0.45 μm filter (Whatman) and the samples were analyzed using an inductively coupled plasma (ICP) optical emission spectrometry (PerkinElmer ICP-Optical Emission Spectrometer Model 8000).

High resolution transmission electron microscope (TEM) images were obtained on a field emission scanning transmission electron microscope (JEOL 2010 F) operating at 200 kV. The sample was prepared by drop-casting a suspension of core–shell catalyst in ethanol on a carbon-coated copper grid and then drying it at ambient condition.

The ζ-potential of NiO nanoparticles in 0.01 M $NaNO_3$ (100 %, Fischer Scientific) at different pH was measured on a Zetasizer Nano ZS (Malvern Instruments). Around 0.8 cm^3 of NiO suspension (1 g L^{-1}) was transferred to a folded capillary zeta cell, DTS1060 (Malvern Instruments). The cell was then inserted into the Nano ZS and the ζ-potential was acquired at ambient temperature.

Powder X-ray diffraction (XRD) measurements were performed on a Bragg–Brentano X-Ray Diffractometer (Rigaku SmartLab) at a 2θ range of 10–80° with a step size of 0.05°, using graphite monochromatic Cu Kα radiation with a nickel filter.

CO-chemisorption was performed on a chemisorption analyzer (ChemBET Pulsar TPR/TPD, Quantachrome). After putting 0.19 g of core–shell nanoparticles into a U-type quartz tube, it was heated up to 650 °C in a He flow of 85 cm^3 STP min^{-1} and then the He stream was switched to 5% H_2/95% Ar (85 cm^3 min^{-1}), followed by holding at 650 °C for 1 h. Subsequently, the 5% H_2/95% Ar stream was switched back to the He stream (50 cm^3 min^{-1}) and the tube was purged for 30 min. Finally, the tube was cooled down to 30 °C. Once the detector signal became stable, successive doses of CO were introduced into the He stream through a calibrated injection loop (0.293 cm^3) until no further CO uptake was detected. In another experiment, the catalyst was pre-reduced at 900 °C in 10% H_2/90% He at 900 °C for 1 h and hereinafter it is referred to as reduced catalyst.

H_2-temperature programmed reduction (H_2-TPR) was carried out on the above chemisorption analyzer. About 10–12 mg of sample was loaded into the quartz tube, and then it was purged with He (85 cm^3 min^{-1}) for 1 h at 140 °C, following by cooling down to 40 °C. Subsequently, the He stream was switched to 5% H_2/95% Ar (85 cm^3 min^{-1}). After maintaining at the above temperature for 45 min, the tube was heated up to 1000 °C at a rate of 5 °C min^{-1}.

2.3. Catalytic testing

Dry reforming of methane was performed on a Setaram SETSYS Evolution thermogravimetric analyzer (TGA) coupled with a MKS Cirrus 2 quadrupole mass spectrometer (MS). About 20 mg of sample was loaded into the quartz cup (0.75 cm^3), it was purged with He (20 cm^3 STP min^{-1}) for 15 min at 20 °C, and then heated up to 600 °C at a rate of 30 °C min^{-1} in a He flow of 270 cm^3 STP min^{-1}. Once the sample temperature reached the target value, a H_2 flow of 30 cm^3 STP min^{-1} was introduced to the He stream and the temperature was held at the above value for 1 h, followed by ramping the sample temperature up to 850 °C at a rate of 30 °C min^{-1} in a He stream (20 cm^3 STP min^{-1}). After the temperature reached the set value, a 26.8% CO_2/26.8CH_4%/46.4% He stream (280 cm^3 STP min^{-1}) was introduced into the above He stream. The concentration of inert, reactants, and products in the effluent stream was monitored by MS. The conversion of methane was calculated from mole fraction of hydrogen in the effluent stream according to Eq. (1), which assumes that only the dry reforming and reverse water–gas shift (RWGS, $H_2 + CO_2 = CO + H_2O$) reactions occur and the molar flowrate of effluent stream is equal to that of reactant stream. The error introduced by the latter assumption is less than 5% because TGA chamber allows poor contact between gas phase and the catalyst and therefore methane conversion is low (less than 10%).

$$X_{CH4} = 100 \times \frac{(y_{H2} + y_{CO})}{(4 \times y_{CH4,0})}\% \quad (1)$$

where X_{CH4} is methane conversion, y_{H2} and y_{CO} are the molar fraction of hydrogen and carbon monoxide in the effluent stream, respectively, and $y_{CH4,0}$ is the mole fraction of methane in the reactant stream (0.25).

After completion of the reaction, the sample was cooled to 20 °C in a He flow of 20 cm^3 STP min^{-1}, followed by holding at this temperature for 12 min. To quantify coke formation, the sample was heated to 900 °C in a He stream (270 cm^3 STP min^{-1}). Once the temperature reached 900 °C, an O_2 flow of 30 cm^3 STP min^{-1} was introduced into the He stream and the sample was kept at this condition for 1.5 h. Finally, the sample was cooled down to 20 °C in a He flow of 20 cm^3 STP min^{-1}.

Dry reforming was also carried out in a fixed-bed reactor (U-type quartz tube, Φ_{in} =4 mm) vertically placed inside an electric furnace. After loading 50 mg core–shell catalyst into the reactor, it was heated in a He flow of 112.5 cm^3 STP min^{-1} to 900 °C at a ramp rate of 10 °C min^{-1}. Once the temperature reached the target value, a H_2 flow of 12.5 cm^3 STP min^{-1} was introduced to the He stream and the temperature was held at the above temperature for 1 h. After that, the reactor was cooled down to 750 °C for 30 min in N_2 (20 cm^3 STP min^{-1}). When the temperature reached 750 °C, a 50% CO_2/50% CH_4 stream (20 cm^3 STP min^{-1}) was introduced to the N_2 stream, resulting in a gas hourly space velocity (GHSV) of 48,000 cm^3 STP $g_{cat}{}^{-1}$ h^{-1}. The catalytic performance was further evaluated at a GHSV of 1524, 000 cm^3 STP $g_{cat}{}^{-1}$ h^{-1} and

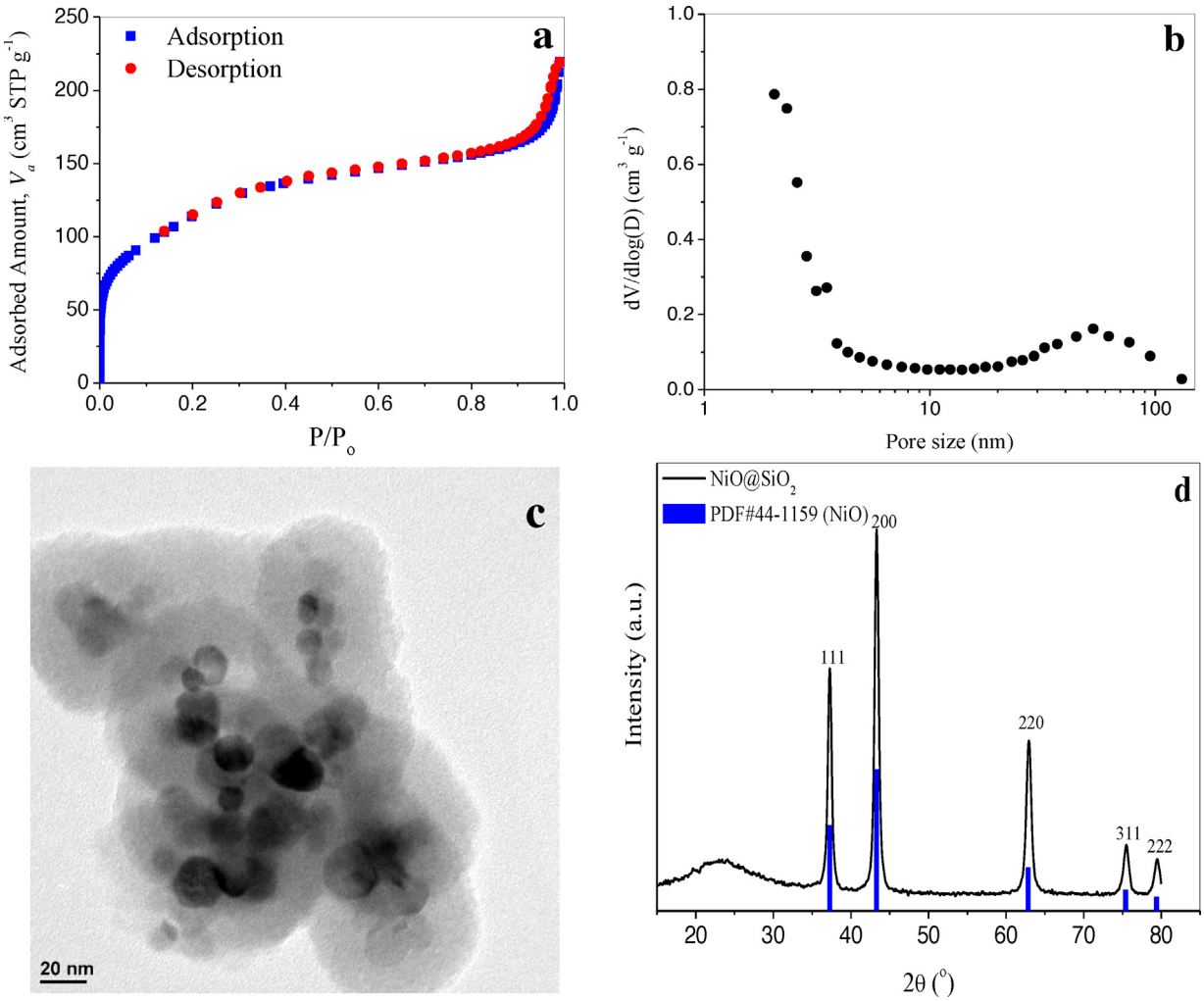

Fig. 1. Physical characterization of calcined NiO@SiO_2 nanoparticles: (a) nitrogen adsorption–desorption isotherms. (b) pore size distribution. (c) TEM images. (d) powder XRD pattern.

750 °C with the same reactant composition. The composition of the effluent stream was continuously monitored by a micro-GC (Agilent CP-490). The conversions of CH_4 and CO_2 were calculated from their molar flow rates at the outlet of reactor.

2.4. Spent catalyst

The spent catalyst recovered from the tubular reactor was characterized by Raman spectroscopy, STEM, N_2-physiorption, CO-chemisorption, and XRD. Raman spectra were acquired on Horiba Jobin Yvon LabRam equipped with a CCD detector and a microscope with a 100 × objective lens. STEM images and mapping were obtained on an Aberration Corrected S/TEM (FEI Titan 80-300) operating at 200 kV. The sample was prepared by drop-casting a suspension of spent catalysts in ethanol on a DuraSiN Film support grid and then drying it at ambient condition. XRD spectra were performed on a Bragg–Brentano X-ray diffractometer (Rigaku SmartLab) at a 2θ range of 10–80° with a step size of 0.05°, using graphite monochromatic Cu Kα radiation with a nickel filter.

The coke content of spent catalyst was estimated from O_2-temperature programmed oxidation (TPO). O_2-TPO was performed on a combined thermogravity-differential scanning calorimeter (Q600, TA Instruments). After loading 18 mg of spent catalyst to sample crucible, the sample and reference crucibles were heated to 900 °C at 10.0 °C min^{-1} in 10 %O_2/90 %Ar (50 cm^3 STP min^{-1}). The molar concentration of CO_2 in the effluent was monitored by MS.

Table 1
N_2–BET and exposed Ni surface area of calcined, reduced and spent core–shell catalyst.

	Calcined	Reduced[a]	Spent[b]
N_2–BET (m^2 g$_{cat.}^{-1}$)	388	221	37
Exposed Ni surface area (m^2 g$_{cat.}^{-1}$)	0.91	0.10	0.10

[a] Reduction in 10% H_2/90% He at 900 °C for 1 h.
[b] Recovered from fixed-bed reactor after DRM at 750 °C for 24.5 h and then burned off coke.

3. Results and discussion

Nitrogen adsorption–desorption isotherms on NiO@SiO_2 calcined at 350 °C (Fig. 1a) exhibit a Type 1 adsorption isotherm in the relative pressure (P/P_o) range of 0–0.8. Such an isotherm is characteristic to microporous materials. The presence of a relatively small Type H1 hysteresis at relative pressures between 0.85 and 1.0 indicates the presence of meso-pores. The N_2 – BET surface area of calcined core–shell particles was found to be 388 m^2 g^{-1} (Table 1). Fig. 1b further illustrates the pore size distribution (PSD) of core–shell particles estimated by applying the Barrett–Joyner–Halenda (BJH) method to the desorption isotherm.

The PSD curve exhibits a narrow distribution at 2 nm or less and a broad peak centered at around 53 nm, clearly indicating a bimodal porosity. The small pores result from the removal of CTAB during calcination, while the large pores may be due to the aggregation of the core–shell particles. For core–shell catalysts, direct access of reactive molecules to the core is of significant importance. This accessibility was evidenced by the CO pulse chemisorption (Fig. S2). Metal surface area was estimated from CO uptake by assuming a CO/Ni stoichiometry of 1.5 and surface Ni atoms density of $1.54 \times 0^{19}\,m^{-2}$. The surface area of Ni was calculated to be $0.91\,m^2\,g_{cat}^{-1}$ (Table 1), notably lower than that for supported Ni catalysts [28]. This low value is partially attributable to SiO_2 overcoating, which may block some metal surface.

To gain more structural information of the core–shell catalyst, we collected TEM images of as-synthesized and calcined core–shell samples. As shown in Fig. 1c, most silica shells contain multiple NiO particles, but in rare cases a single NiO particle is encapsulated within a silica shell (Fig. S3). The presence of multiple NiO cores within a single enclosed shell results from the relatively poor dispersion of the commercial NiO NPs in the CTAB solution. Better dispersion of commercial NPs could be achieved using other surfactants (e.g., tetradecyltrimethylammonum bromide), decreasing the concentration of NiO, or both. A closer examination of TEM images reveals that the average thickness of silica shells surrounding NiO NPs is around 20 nm. Energy dispersive X-ray (EDX) spectroscopy data suggests that NiO content of calcined core–shell catalyst is 36.9 wt.%, which corresponds to 31.5 wt.% Ni in the reduced catalyst if all NiO is completed reduced. This value is very close to the one (38.5 wt.% NiO in the calcined catalyst) determined by ICP measurements. The formation of the silica shell is

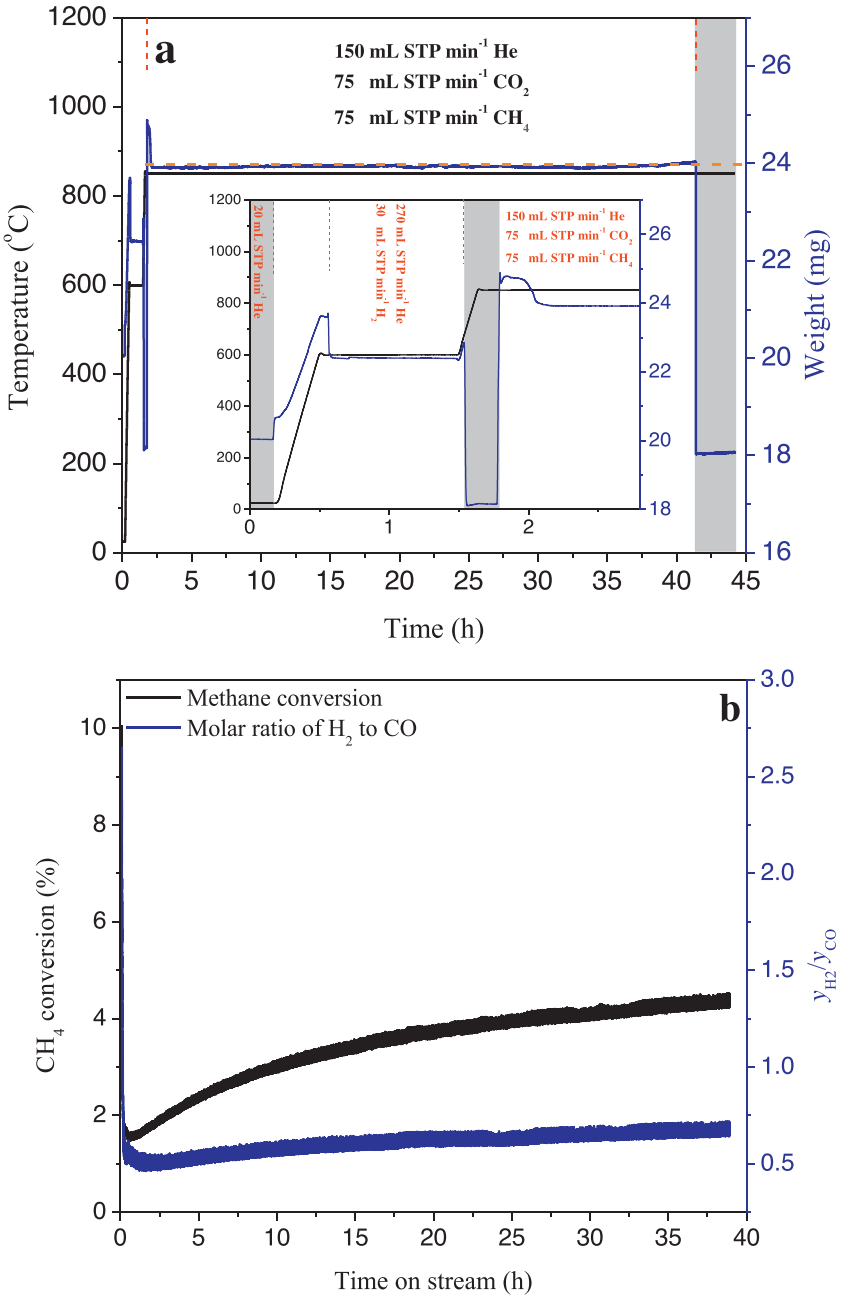

Fig. 2. Dry reforming of methane with carbon dioxide over Ni@SiO_2 on a therogravimeter: (a) sample weight as a function of time (inset the weight profile in the first 2.8 h). (b) CH4 conversion and molar ratio of H_2/CO in the product stream.

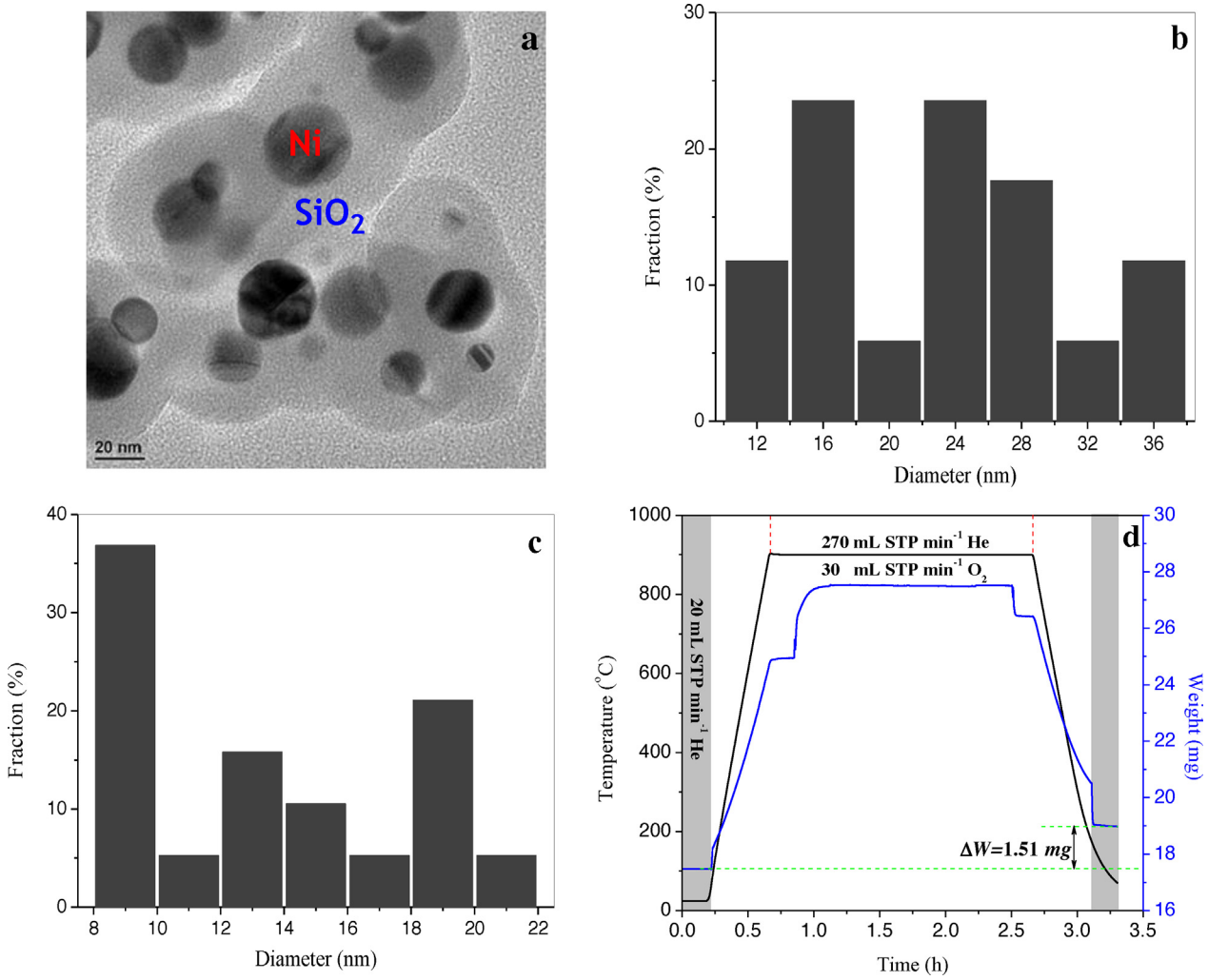

Fig. 3. Characterization of used Ni@SiO2 catalyst after 39 h test at 850 °C and calcined catalyst: (a) in-situ oxidation. (b) TEM image. (c) Ni size distribution of spent catalyst. (d) NiO size distribution of calcined catalysts.

induced by the electrostatic interaction between negative charged silicate species and surfactant cations (CTA+) under basic conditions. The surfactant cation (headgroups) adsorb on NiO particles via a bromide anion (Br^-), serving as the mediator for bonding two positive bodies, which are positive at pH below 11 (Fig. S4). In this case, one expects that an outer layer of surfactants forms around the inner layer by hydrophobic force with the headgroup pointing toward the bulk aqueous phase. The bilayer of CTAB not only stabilizes NiO nanoparticles in water but also acts as a template for polymerization of silicate. After tetraethyl orthosilicate (TEOS) molecules are added to the basic solution, they first hydrolyze and then condense, producing negatively charged oligomeric silica species. These species are attracted to the surface of outer surfactant layer, from which condensation proceeds until no TEOS molecules are available. Subsequently, the surfactant molecules are removed through calcination, producing a porous silica layer. The silica shell is amorphous, as confirmed by XRD spectra (Fig. 1d). XRD spectra also indicate that the crystal structure of NiO NPs remains unchanged.

Catalytic performance of Ni@SiO_2 catalyst toward DRM was first evaluated using a TGA. After loading the catalyst into a quartz cell that is suspended inside the TGA chamber, the sample was reduced in a stream of 10% H_2 balance He for 1 h at 600 °C, followed by ramping the sample temperature up to 850 °C in He. Once the desired temperature is reached, a stream of 26.8% CO_2/26.8% CH_4/46.4% He was fed to the chamber. The drastic change in sample weight accompanying gas switching, as shown in Fig. 3a, is caused by gas drag effects. Decrease in sample weight at 600 °C results from NiO reduction. At 850 °C, feeding the stream that contains CO_2 and CH_4 to the TGA chamber gives rise to a spike which is followed by a rapid increase on the sample weight profile. Subsequently, the sample weight deceases from 24.8 to 23.9 mg in 20 min and then remains almost unchanged (in 39 h) until the end of run (Fig. 2a). No further weight change is due to the absence of coke deposition, because both CH_4 conversion (above 1.5%) and the molar ratio of H_2 to CO in the effluent stream indicate that Ni@SiO_2 exhibits notable catalytic activity toward DRM (Fig. 2b). In 39 h on stream, the average CH_4 conversion in 39 h is 3.3%. In contrast, methane conversion over reduced bare NiO NPs is less than 0.15% under the same conditions (Fig. S5) and coke deposition is negligible, suggesting bare nickel particles have no activity toward either reforming or decomposition. This may result from sintering of uncoated Ni nano-particles. For a Ni-based steam reforming catalyst (HiFUELTM R110, Alfa Aesar), more than 0.32 g (coke) g^{-1} (reduced catalyst) is produced during a reaction period of 6.4 h under the same reaction conditions (Fig. S7).

Fig. 2b exhibits that CH_4 conversion increases monotonically to 4.4% after it reaches a minimum of 1.5% (ca. 45 min after feeding CH_4 and CO_2) as the reaction proceeds. One factor contributed to the decreasing activity in the first 45 min of reforming could be

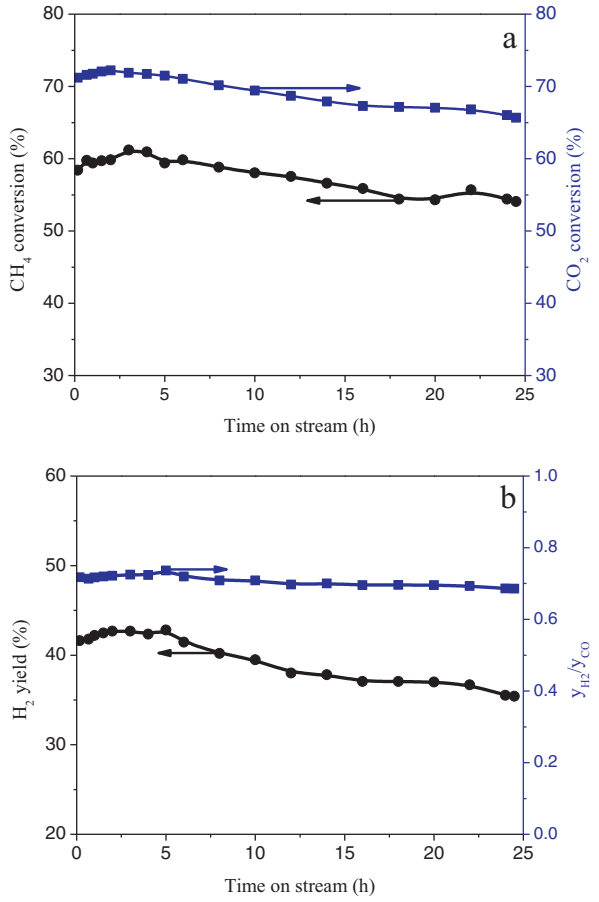

Fig. 4. Long-term catalytic performance of Ni@SiO_2 in a fixed-bed reactor: (a) CH_4 and CO_2 conversions and (b) H_2 yield and H_2/CO molar ratio. (T = 750 °C, P = 0.1 MPa, GHSV = 48,000 $cm^3\ g_{cat.}^{-1}\ h^{-1}$, CH_4:CO_2:N_2 = 1:1:2).

the loss of exposed Ni surface area, as revealed by the TEM images of spent catalysts after DRM testing (Fig. 3a). For the spent catalyst, around 60% of Ni NPs are larger than 20 nm, and some Ni NPs are as big as 40 nm (Fig. 3b). While for the calcined (unreduced) catalyst, almost all NPs are less than 20 nm (Figs. 1c and 3c). This observation, together with the round shape of large Ni NPs inside the shell, exhibits that the sintering occurs inside the shell that contains multiple NPs. Because Tammann temperature ($0.5T_m$) of nickel is 590 °C, agglomeration of Ni NPs inside the silica shell can be significant at temperatures above 650 °C. As the temperature increases, sintering leads to rapid loss of metal surface area. After reducing the core–shell catalyst at 900 °C for 1 h in H_2, exposed Ni surface area decreases from 0.91 to 0.1 $m^2\ g_{cat}^{-1}$ (Table 1). On the other hand, the shell appears to remain intact. Therefore, the Ni core maintains its relatively stable catalytic activity toward DRM. The increased DRM reactivity before it reaches a steady state has also been reported for silica coated Ni/SiO_2 [21] and alumina coated Ni/Al_2O_3 [29]. Tentatively, this transition period is attributed to the structural change of silica shell as revealed by the N_2–BET measurements (Table 1), the decreased mass transfer resistance in the TGA crucible, or both.

After reforming for ~39 h at 850 °C, the reactant stream was switched to the He stream (20 cm^3 STP min^{-1}) and we found that the weight of spent catalyst (18.06 mg) is very close to that of freshly reduced catalyst (18.15 mg), indicating carbon deposition on the core–shell catalyst is negligible. Therefore, the in-situ oxidation of spent (fully reduced) catalyst can be used to accurately estimate the Ni content of core–shell catalyst. Fig. 3d shows that the sample weight increases by 1.51 mg after the spent catalyst was oxidized, corresponding to a Ni loading of 31.7 wt.% in the reduced catalyst (17.48 mg at room temperature in 20 cm^3 STP min^{-1} He). This value is comparable with estimations from EDX (31.5 wt.%) and IPC measurements (32.8 wt.%).

To further evaluate the performance of Ni@SiO_2 catalyst, the reforming reaction is conducted at 750 °C in a continuous flow, fixed-bed reactor coupled with GC. A lower reaction temperature is selected because coke formation is more thermodynamically favored with decreasing reaction temperature [29]. Before feeding reactants to the reactor, the catalysts were reduced at 900 °C for 1 h to provide additional thermal stability for the catalyst under the reforming temperature. We found that the initial CO_2 and CH_4 conversions are 71.2% and 58.4%, respectively (Fig. 4a). As Fig. 4a shows, both CO_2 and CH_4 conversions increase slightly in the first 2.5 h and then decrease to 65.6% and 54.1%, respectively, after 24.5 h on stream. At 750 °C, the average turnover frequency (TOF) of methane is 33.4 s^{-1} (Table 2), which is notably higher than that on immobilized Ni NPs (0.31 s^{-1} at 750 °C [20]) and Ni/SiO_2@SiO_2 (8.22 s^{-1} at 800 °C [21]) which is obtained at low space velocities, but lower than that over Ni–Yolk@Ni@SiO_2 nanocomposite (85.8 s^{-1} at 800 °C [19]). At a GHSV of 1524 L STP $g_{cat}^{-1}\ h^{-1}$, the TOF of CH_4 is above 182 s^{-1} (Table 2 and Fig. S8) [19]. Generally, the TOF of CH_4 mainly depends on the reaction temperature. However, it can also be affected by space velocity if diffusion effects are significant [30]. Therefore, direct comparisons of methane conversion rates among different studies only provide a preliminary evaluation of catalyst activities. However, it does appear that the TOF of CH_4 over coated Ni NPs is higher than that over supported Ni NPs [19–21,31,32]

Based on Gibbs energy minimization via ASPEN Plus® simulation, equilibrium conversions of CH_4 and CO_2 are 96 and 84%, respectively and H_2/CO ratio is 1.16 at 750 °C. Thus, the effluents from the fixed-bed reactor are not equilibrated. Both hydrogen yield and H_2/CO ratio follow a similar trend as conversions (Fig. 4b). One interesting finding is that H_2/CO ratio is below 0.75, which is due to RWGS reaction. These results may suggest that RWGS reaction becomes more important as the DRM activity decreases, which causes H_2 yield to drop at a slightly faster rate than CH_4 conversion (Fig. 4b). Insights into the slow decrease in catalytic activity were provided by the characterization of spent catalyst.

TPO profile of the spent catalyst after DRM test is shown in Fig. 5a. By integration of CO_2 flowrate, the coke content is found to be 1.2 wt.%. In contrast, the reactor was plugged with coke when using HiFUELTM R110 as the reforming catalyst at identical operating conditions. On the TPO curve, there is only one peak between 100 and 900 °C, which can be deconvoluted into two Gaussian subpeaks at 530 °C (area fraction is 0.64) and 625 °C (0.36),

Table 2
Comparison of methane conversion rates among different studies.

	T (°C)	GHSV (L $g_{cat}^{-1}\ h^{-1}$)	$x_{CH4,0}$	X_{CH4} (%)	Ni_w (wt.%)	$Ni_{surface}$ (μ mol g_{cat}^{-1})	CH_4 conversion rate (mol $g_{cat}^{-1}\ s^{-1}$)	(mol $g_{Ni}^{-1}\ s^{-1}$)	TOF
Ref. [19]	800	1440	0.33	10	18.6	6.94	5.95×10^{-4}	3.20×10^{-3}	85.8
Ref. [20]	750	7.5	0.5	96	6.1	147	4.46×10^{-5}	7.32×10^{-4}	0.31
Ref. [21]	800	4	0.45	42	N/A	1.16	9.38×10^{-6}	N/A	8.22
This work	750	48	0.25	57.5	29	2.56	8.56×10^{-5}	2.82×10^{-4}	33.4
This work	750	1524	0.25	11.3	29	2.56	5.13×10^{-4}	1.69×10^{-3}	182

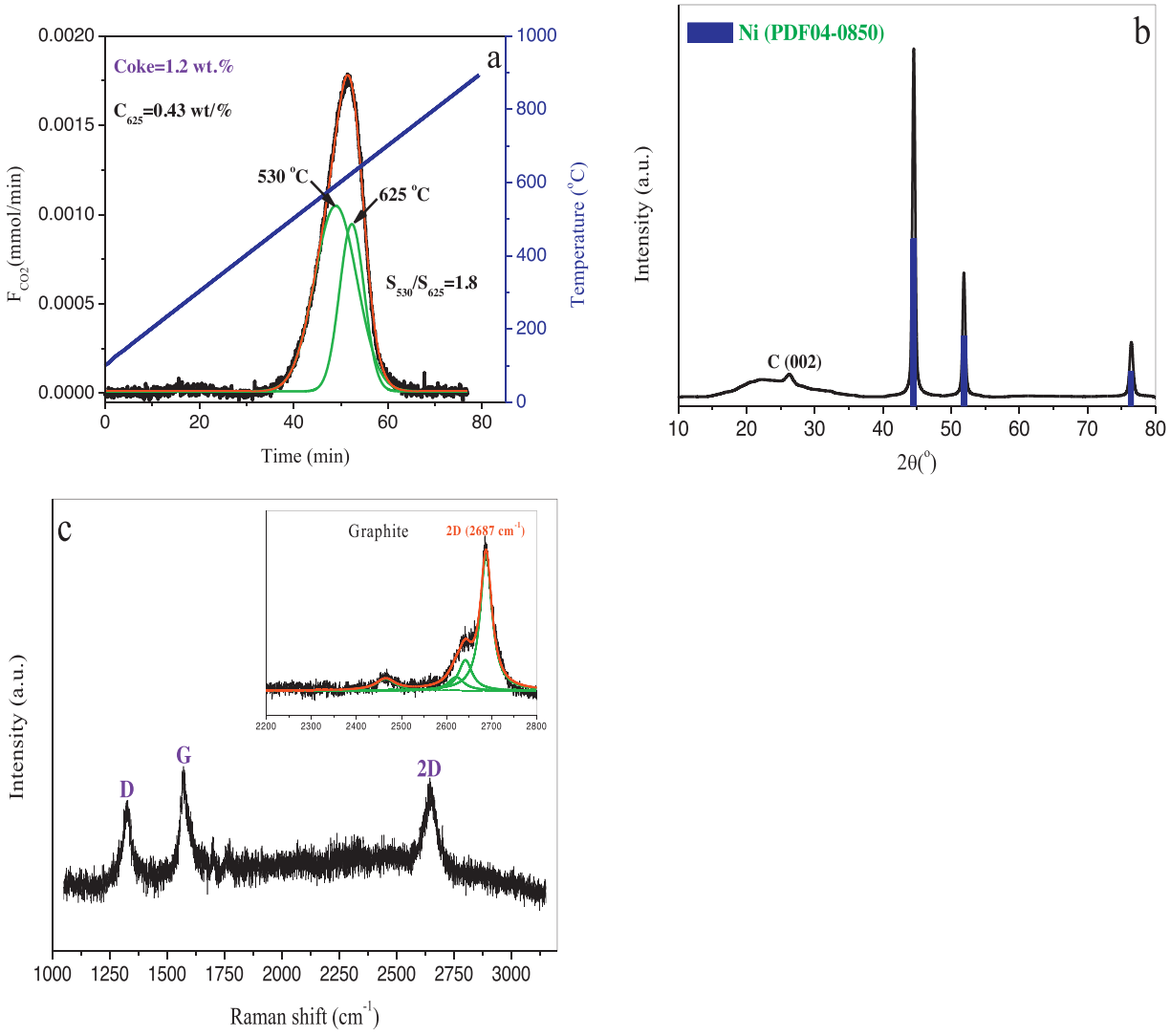

Fig. 5. Characterization of spent Ni@SiO_2 catalyst after 24.5 h test at 750 °C: (a) CO_2 profile of TPO, (b) XRD pattern, and (c) Raman spectra (inset is the spectrum of graphite).

indicating two types of coke in the spent catalyst. Several types of coke have been identified in hydrocarbon reactions over nickel, they are adsorbed atomic carbon (C_α), polymeric, amorphous carbon (C_β), whisker carbon (C_ν), nickel carbide (C_γ), and graphitic carbon (C_c) [33]. Among them, C_α can be easily gasified and C_c is difficult to gasify [34]. The subpeak at 625 °C is assigned to graphitic carbon, and its content is 0.43 wt.%. The subpeak at 530 °C is assigned to amorphous carbon. The occurrence of graphitic carbon is confirmed by the XRD pattern (Fig. 5b). The small diffraction peak at 26.3° is attributed to (0 0 2) plane of hexagonal graphite structure, where the other three strong and sharp peaks (44.6°, 51.9°, and 76.4°) correspond to (1 1 0), (2 0 0), and (2 2 0) planes of face-centered cubic nickel structure (PDF #04-0850). No additional crystalline phases are detected in the spent catalyst. The presence of coke is also revealed by the Raman spectroscopy (Fig. 5c). The Raman spectrum of spent catalyst displays three main peaks at 1325, 1569, and 2650 cm^{-1}, which are assigned to D, G and 2D bands of carbon-based materials, respectively. However, both the position and the shape of 2D band for spent catalyst is different from those for graphite, suggesting that the coke may exist in the form of graphite nanoplatelets. Further information about the spatial distribution of C and Ni in the spent catalyst was provided by STEM-EDX mapping (Fig. 6). The elemental maps suggest that coke partially covers certain areas of Ni surface, causing slow deactivation. In addition, no filamentous carbon can be observed in the STEM image. This may indicate that the size of the voids inhibits the formation of carbon filaments, which are typically tens of nanometers in diameter [9,11,35,36]. It was reported that densification of porous shell, if occurs in DRM, has little effect on the activity [21]. The N_2-phsyisorption measurements clearly demonstrate that porous structure of silica shell collapses during reduction and reforming (Table 1). The N_2–BET surface area of reduced and spent catalysts are 221 and 37 $m^2\ g_{cat}^{-1}$, which are much lower than that of calcined catalyst (388 $m^2\ g_{cat}^{-1}$). The same phenomenon was also reported for other core–shell catalysts [19,21]. This may result from the instability of silica shell under the high reaction temperature, especially in the presence of steam product at high temperatures [37]. However, the exposed Ni surface area remains unchanged during the reforming reaction (Table 1). Based on N_2-physisorption and CO-chemisorption, we conclude that the decrease in the reforming activity arises from coke deposition as opposed to loss of metal surface area.

For Ni@SiO_2 catalyst prepared from NiO NPs, reduction of NiO cores generates nanocavities that locate between the core surface and the inner wall of shells (Fig. 5d), which were also observed in previous studies [19,26]. Therefore, coke could form in these cavities, as revealed by Fig. 5d. The observation is consistent with a previous report for silica coated nickel NPs in POM [26]. Due to

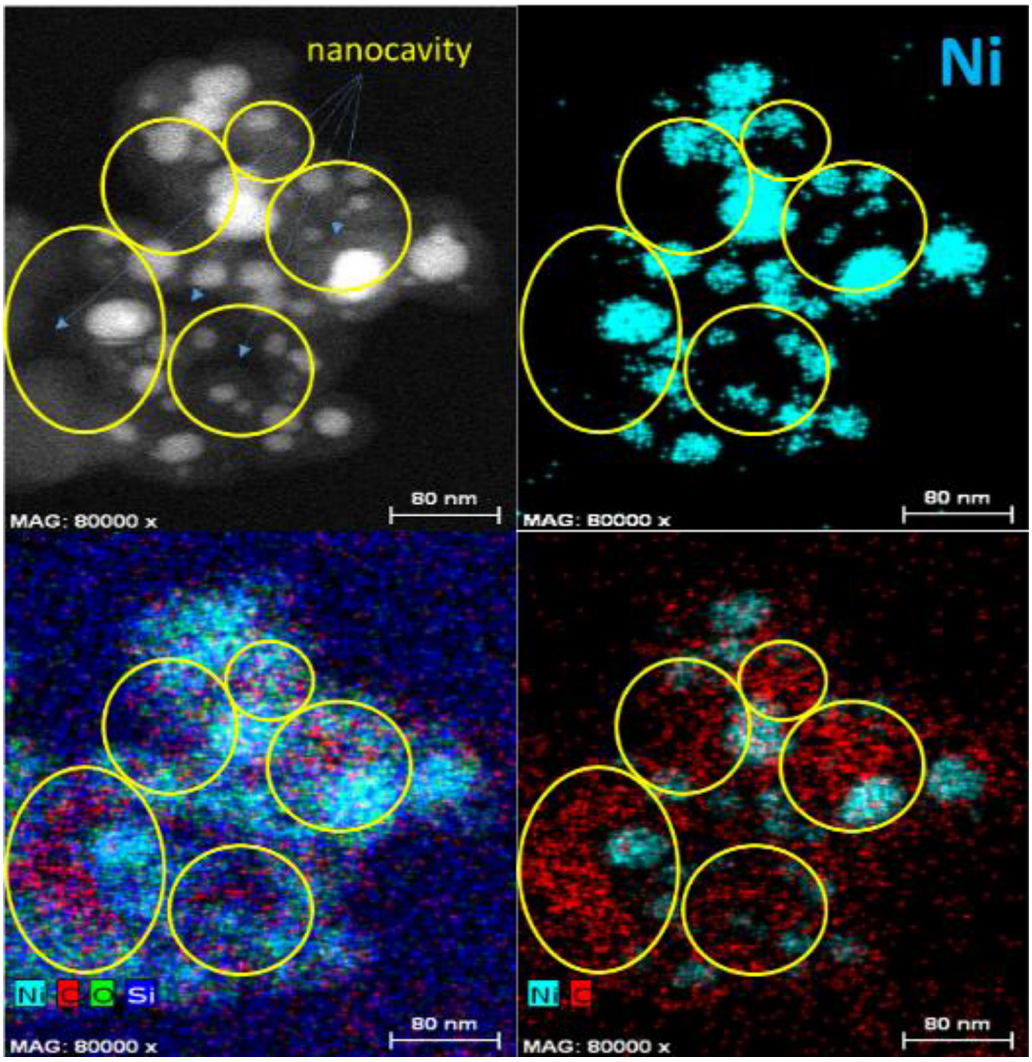

Fig. 6. STEM images and EDX mapping of spent Ni@SiO2 catalyst after 24.5 h test at 750 °C. STEM image and EDX maps.

the steric effect, however, the formation of carbon filaments inside the nanocavities is inhibited. A recent work reported that coking is negligible in the nanocavities of Ni@SiO_2 in DRM. However, this conclusion was drawn on the basis of TGA data [19], which cannot provide a good estimate of coke content because both oxidation of nickel and coke gasification lead to sample weight change (Fig. S9). Based on the above findings, we surmise silica coating can effectively inhibit the formation of filamentous carbon on nickel surface during DRM reactions. The presence of nano-sized cavities between reduced NiO nano-particles and silica shell, however, can allow the formation of amorphous carbon and graphite nanoplatelets. Strategies for further improving the coke-resistance would hinge upon reduction of the nano-cavities. This can be achieved by using Ni nanoparticles and calcination under a reducing environment, improvements of nanoparticle dispersion, and/or passivating the active sites for coke formation.

4. Conclusions

In summary, we demonstrated that core–shell NiO@SiO_2 nanoparticles can be fabricated from NiO NPs by a facile method in three steps: (i) dispersing NiO NPs into CTAB solution by using a high-speed blender; (ii) growing a silica shell around the nanoparticle by a sol–gel process; (iii) removing surfactant molecules by calcination. After calcination in static air, both micropores and mesopores are created in the amorphous silica shell. These pores serve as channels through which gas molecules diffuse, and the shell suppresses carbon filament growth. The core–shell catalyst exhibits excellent catalytic performance toward dry reforming of methane with carbon dioxide. On a thermogravimeter, coke deposition is negligible in 39 h on stream at 850 °C. In a continuous flow, fixed-bed reactor, the core–shell catalyst maintains a relatively high stability in 24.5 h on stream. The coke content of spent catalyst is estimated to be 1.2 wt.%. Two types of coke, i.e., amorphous carbon and graphite nanoplatelets, have been identified. The core–shell structure is thermally stable at reaction temperatures investigated (up to 850 °C). The porous silica shell significantly suppresses sintering and coking; thus, the coated nickel cores have high stability and activity. The catalytic performance of Ni@SiO_2 catalysts can be further improved by tuning the microstructure of core–shell nanoparticles and surface of Ni NPs inside the shell. With enhanced sintering and coke resistance and facile synthesis method, the reported core–shell Ni catalyst can potentially be applied for a number of high-temperature hydrocarbon reactions.

Acknowlegdements

The work was supported by the U.S. National Science Foundation under award (CBET-1254351) and North Carolina State University Start-Up Funds. The authors are grateful to S. T. Thompson and Prof.

Lamb for N_2-physisorption measurements at North Carolina State University. We also would like to thank A. Shafiefarhood for collecting TEM images and D. Bhuana and N. Galinsky for acquiring XRD spectra.

Appendix A. Supplementary data

Supplementary data associated with this article can be found, in the online version, at http://dx.doi.org/10.1016/j.apcatb.2015.04.039.

References

[1] M.C. Bradford, M.A. Vannice, Catal. Rev. Sci. Eng. 41 (1999) 1–42.
[2] A.T. Ashcroft, A.K. Cheetham, M.L.H. Green, P.D.F. Vernon, Nature 352 (1991) 225–226.
[3] A. Erdöhelyi, J. Cserenyi, F. Solymosi, J. Catal. 141 (1993) 287–299.
[4] J.R. Rostrup-Nielsen, J.H.B. Hansen, J. Catal. 144 (1993) 38–49.
[5] A.M. Gadalla, B. Bower, Chem. Eng. Sci. 43 (1988) 3049–3062.
[6] M.C.J. Bradford, M.A. Vannice, Appl. Catal. A 142 (1996) 73–96.
[7] A.N. Fatsikostas, X.E. Verykios, J. Catal. 225 (2004) 439–452.
[8] S. Sokolov, E.V. Kondratenko, M.M. Pohl, A. Barkschat, U. Rodemerck, Appl. Catal. B 113–114 (2012) 19–30.
[9] K. Mette, S. Kühl, H. Düdder, K. Tarasov, M. Muhler, ChemCatChem 6 (2014) 100–104.
[10] H.S. Bengaard, J.K.N. Nørskov, J. Sehested, B.S. Clausen, L.P. Nelsen, A.M. Molenborek, J.R. Rostrup-Neilsen, J. Catal. 209 (2002) 365–384.
[11] S. Helveg, C. Lopez-Cartes, J. Sehested, P.L. Hansen, B.S. Clausen, J.R. Rostrup-Nielsen, F. Abild-Pedersen, J.K. Norskov, Nature 427 (2004) 426–429.
[12] R. Pereñiguez, V.M. Gonzalez-delaCruz, A. Caballero, J.P. Holgado, Appl. Catal. B 123–124 (2012) 324–332.
[13] S. Zhang, S. Muratsugu, N. Ishiguro, M. Tada, ACS Catal. 3 (2013) 1855–1864.
[14] J.R. Rostrup-Nielsen, J. Catal. 85 (1984) 31–43.
[15] C. Liu, J. Ye, J. Jiang, Y. Pan, ChemCatChem 3 (2011) 529–541.
[16] X. Xie, T. Otremba, P. Littlewood, R. Schomäcker, A. Thomas, ACS Catal. 3 (2013) 224–229.
[17] T.H. Cardner, J.J. Spivey, E.L. Kugler, D. Pakhare, Appl. Catal. A 455 (2013) 129–136.
[18] X. Du, D. Zhang, R. Gao, L. Huang, L. Shi, J. Zhang, Chem. Commun. 49 (2013) 6770–6772.
[19] Z. Li, L. Mo, Y. Kathiraser, S. Kawi, ACS Catal. 4 (2014) 1526–1536.
[20] T. Xie, L. Shi, J. Zhang, D. Zhang, Chem. Commun. 50 (2014) 7250–7253.
[21] J.W. Han, C. Kim, J.S. Park, H. Lee, ChemSusChem 7 (2014) 451–456.
[22] S.H. Joo, Y.Y. Park, C.K. Tsung, Y. Yamada, P. Yang, G.A. Somorjai, Nat. Mater. 23 (2009) 126–131.
[23] J. Lu, B. Fu, M.C. Kung, G. Xiao, J.W. Elam, H.H. Kung, P.C. Stari, Science 335 (2012) 1205–1208.
[24] M. Cargnello, J.J.D. Jaén, J.C.H. Garrido, K. Bakhmutsky, T. Montini, J.J.C. Gámez, R.J. Gorte, P. Fornasiero, Science 227 (2012) 713–717.
[25] Z. Li, Y. Kathiraser, J. Ashhok, U. Oemar, S. Kawi, Langmuir 30 (2014) 14694–14705.
[26] S. Takenaka, H. Umebayashi, E. Tanabe, H. Matsune, M. Kishida, J. Catal. 245 (2007) 392.
[27] L. Li, S. He, Y. Song, J. Zhao, W. Ji, C.T. Au, J. Catal. 288 (2012) 54–64.
[28] R. Geyer, J. Hunold, M. Keck, P. Kraak, A. Pachulski, R. Schödel, Chem. Ing. Tech. 84 (2012) 160–164.
[29] T.D. Gould, A. Izar, A.W. Weimer, J.L. Falconer, J.W. Medlin, ACS Catal. 4 (2014) 2714–2717.
[30] M.K. Nikoo, N.A.S. Amina, Fuel Process. Technol. 92 (2011) 678–691.
[31] Y. Wang, H. Liu, B. Xu, J. Mol. Catal. A 299 (2009) 44–52.
[32] N. Wang, K. Shen, Li Huang, X. Yu, W. Qian, W. Chu, ACS Catal. 3 (2013) 1351–1638.
[33] C.H. Bartholomew, Appl. Catal. A 212 (2001) 17–60.
[34] J.M. Thomas, W.J. Thomas, Principles and Practice of Heterogeneous Catalysis, Wiley-VCH, Weinheim, 1997.
[35] E. Boellaard, P.K.D. Bokx, A.J.H.M. Kock, J.W. Geus, J. Catal. 96 (1985) 481–490.
[36] V.Y. Bychkov, Y.P. Tyulenin, A.A. Firsova, E.A. Shafranovsky, A.Y. Gorenberg, V.N. Korchak, Appl. Catal. A 453 (2013) 71–79.
[37] A. Corma, Chem. Rev. 97 (1997) 2373–2419.